




Marine volcanoclastic record of early arc evolution in the eastern Ritter Range pendant, central Sierra Nevada, California

Barth, A.P.¹ , Wooden, J.L.², Riggs, N.R.³, Walker, J.D.⁴ , Tani, K.⁵, Penniston–Dorland, S.C.⁶, Jacobson, C.E.⁷ , Laughlin, J.A.¹, Hiramatsu, R.¹

¹Department of Earth Sciences, Indiana University~Purdue University Indianapolis, Indianapolis, IN 46202

²U.S. Geological Survey, Menlo Park, CA (retired)

³School of Earth Sciences and Environmental Sustainability, Northern Arizona University, Flagstaff, Arizona 86011

⁴Department of Geology, University of Kansas, Lawrence, Kansas 66045

⁵National Museum of Nature and Science, Tokyo, Japan

⁶Department of Geology, University of Maryland, College Park, MD 20742

⁷Department of Earth and Space Sciences, West Chester University, West Chester, PA 19383, and Department of Geological and Atmospheric Sciences, Iowa State University

Key Points:

- Detrital zircons preserve age and trace element evidence of ignimbrite provenance
- Zircons record >50 million years of early arc magmatic pulses and lull
- Explosive volcanism and batholith construction were closely coupled at million-year time scales

ABSTRACT

Marine volcanoclastic rocks in the Sierra Nevada preserve a critical record of silicic magmatism in the early Sierra Nevada volcanic arc, and this magmatic record provides precise minimum age constraints on subduction inception and tectonic evolution of the early Mesozoic Cordilleran

This is the author's manuscript of the article published in final edited form as:

Barth A.P., Wooden J.L., Riggs N.R., Walker J.D., Tani K., Penniston–Dorland S.C., ... Hiramatsu R. (2018). Marine Volcanoclastic Record of Early Arc Evolution in the Eastern Ritter Range Pendant, Central Sierra Nevada, California. *Geochemistry, Geophysics, Geosystems*, 0(ja). <https://doi.org/10.1029/2018GC007456>

convergent margin at this latitude. New zircon Pb/U ages from the Ritter Range pendant and regional correlations indicate arc inception no later than mid-Triassic time between 37 and 38°N. The regional first-order felsic magma eruption rate as recorded by marine volcanic arc rocks was episodic, with distinct pulses of ignimbrite emplacement at ca. 221 to 216 Ma and 174 to 167 Ma. Ignimbrites range from dacite to rhyolite in bulk composition, and are petrographically similar to modern arc-type, monotonous intermediate dacite or phenocryst-poor, low-silica rhyolite. Zircon trace element geochemistry indicates that Jurassic silicic melts were consistently Ti- and light rare earth-enriched and U-depleted in comparison to Triassic melts of the juvenile arc, suggesting Jurassic silicic melts were hotter, drier, and derived from distinct lithospheric sources not tapped in the juvenile stage of arc construction. Pulses of ignimbrite deposition were coeval with granodioritic to granitic components of the underlying early Mesozoic Sierra Nevada batholith, suggesting explosive silicic volcanism and batholith construction were closely coupled at one- to two-million-year time scales.

Index Terms: 1165, 1065, 8185

INTRODUCTION

The destruction of oceanic lithosphere by subduction leads to the growth of volcano-plutonic arcs and is a major process of tectonic and chemical evolution of the Earth. Marine sedimentary records of arc volcanism can provide insight into the evolutionary history of subduction inception, tectonic evolution of a new and evolving convergent margin, and surficial magmatic processes early in the generation of new continental crust (Gill et al., 1994; Reagan et al., 2010; Ishizuka et al., 2011; Arculus et al., 2015; Straub et al., 2015). Variation in arc magma compositions may record changes in slab inputs and/or overriding-plate lithospheric structure as the juvenile volcanic arc matures.

Early Cordilleran magmatic arc volcanic rocks and broadly contemporaneous batholithic rocks are widely exposed in the central Sierra Nevada of California (Bateman, 1992). Intra-batholithic pendants in the eastern high Sierra (Figure 1) preserve stratigraphic sections rich in volcanic rocks that record the most complete and prolonged record of volcanic arc inception and evolution in this continent-fringing volcanic arc setting. Studies of these incompletely preserved volcanic sections are critically important to understanding juvenile volcanic arc evolution and potential linkages between explosive volcanism and assembly of the underlying batholith. Geochemical and geochronological studies of the Sierra Nevada magmatic arc suggest a complex relationship between volcanism and batholith construction that remains controversial and poorly constrained (Kistler and Swanson, 1981; Busby-Spera, 1984; Saleeby et al., 1990; Glazner, 1991; Bateman, 1992; Fiske and Tobisch, 1994; Tobisch et al., 2000; Barth et al., 2012, 2013).

Magmatic zircons in arc volcanoclastic rocks provide coupled temporal and geochemical records of silicic melt evolution that complement whole rock analyses and resist the effects of hydrothermal alteration and subsequent metamorphism. In this study we use geochronology and geochemistry of zircons in tuffs to decipher the temporal evolution of the Sierra marine volcanic arc from inception through its first ~80 m.y. of magmatism. We report seventeen new Pb/U zircon ages and associated whole rock and zircon geochemistry for dacitic to rhyolitic ignimbrite marker units from the eastern Ritter Range pendant and adjacent Mount Morrison pendant in the east-central Sierra Nevada (Figures 1 and 2). By their nature, felsic ignimbrites provide only a partial record of arc volcanism, but these tuffs provide consistently datable horizons for constraining both the timing of deposition and the subsequent structural evolution of

stratigraphic sequences in Sierran pendants. In addition, whole rock and zircon geochemistry of tuffs provides insight into silicic volcanic rocks compositionally akin to voluminous Mesozoic granodioritic to granitic batholithic rocks. Comparison of ages and compositions of felsic ignimbrites in the Ritter Range and adjacent pendants with the geochronology and geochemistry of intrusive suites exposed beneath volcanic sequences provides temporal control and petrologic evidence for links between explosive felsic arc volcanism and early arc batholith construction (Chen and Moore, 1982; Saleeby et al., 1990; Bateman, 1992; Barth et al., 2011, 2012).

GEOLOGIC SETTING

Marine arc inception and early arc evolution are recorded in both plutonic and volcanic rocks in the Sierra Nevada of east-central California. The Triassic Scheelite and Jurassic Palisade Crest Intrusive Suites are exposed in the eastern range front of the central Sierra Nevada and in adjacent ranges to the east (Sawka et al., 1990; Bateman, 1992; Mahan et al., 2003; Barth et al., 2011). Along the western margin of these intrusive suites, the Saddlebag Lake, Ritter Range and Mount Morrison pendants preserve early Mesozoic marine volcanic rocks, including widespread ignimbrites of Triassic and Jurassic age interbedded with lava flows, breccias, and bedded tuffs (Fiske and Tobisch, 1978; Kistler and Swanson, 1981; Sorensen et al., 1998; Schweickert and Lahren, 1993, 2006). Volcanic and volcanoclastic rocks were emplaced in a marine setting, as evidenced by interbedded marine limestones in some locations and delicate hyaloclastic textures in others (Fiske and Tobisch, 1978; Roberts et al., 2011; Fields et al., 2017). Although recent marine eruptions of large-volume ignimbrites have not been documented, caldera formation in subaqueous settings has been common in young arcs such as Izu-Bonin (Fiske et al., 2001; Tani et al., 2008; Tamura et al., 2009), Kermadec (Lloyd et al., 1996; Wright et al., 2003), and

southwest Japan (e.g., Aira caldera; Aramaki, 1984). Dateable ignimbrites occur 50 meters or less above the base of the exposed volcanoclastic section in the Saddlebag Lake and Ritter Range pendants; ages of ignimbrites thus represent precise but minimum age constraints for inception and record explosive silicic magmatic evolution of a long-lived marine arc at this latitude.

Structural and stratigraphic studies in arc volcanic rocks exposed in east Sierra pendants have suggested a broadly three-stage history of the Mesozoic volcanic arc, with early marine arc deposition of volcanoclastic rocks and lavas and later regional shortening and tilting in Late Jurassic and/or Early Cretaceous time, followed by renewed deposition in Cretaceous time in a subaerial arc setting (Fiske and Tobisch, 1978, 1994; Tobisch et al., 1977, 1986, 2000; Sorensen et al., 1998; Schweickert and Lahren, 1999). Most pendants preserve only part of this three-stage Mesozoic history, but one of the best-exposed and continuous records is represented by volcanic and volcanoclastic rocks of the Saddlebag and Ritter Range pendants (Tobisch et al., 2000; Schweickert and Lahren, 2006). The stratigraphic sequence in these pendants is the most continuous record of the Sierra Nevada volcanic arc, but recovering this record requires accounting for the effects of hydrothermal alteration, flattening and imbrication by thrusting, and a low P/T metamorphic overprint associated with later Mesozoic plutonism (Hanson et al., 1993; Sorensen et al., 1998).

The composite section of metamorphosed Mesozoic volcanic rocks in the eastern Sierra Nevada belongs to the Koip sequence (Kistler, 1966a, b; Kistler and Swanson, 1981; Bateman et al., 1983), unconformably overlying Paleozoic to early Triassic metasedimentary rocks of the distal Cordilleran passive margin (Stevens and Greene, 1999, 2000; Figures 3 and 4). In the Saddlebag

Lake pendant, 232 to 219 Ma silicic ignimbrites are intercalated with andesitic dome facies and metasedimentary rocks in an imbricated section (Schweickert and Lahren, 2006; Barth et al., 2011, 2012; Savage et al., 2017). This volcanoclastic section extends southward into the eastern Ritter Range pendant (Huber and Rinehart, 1965), where metavolcanic rocks are predominantly tuff, lapilli tuff, tuff breccia, and lavas, with prominent marker units of ignimbrite that range from <1 m to ~350 m in thickness (Tobisch et al., 1977; Hanson et al., 1993; Sorensen et al., 1998). Thin intercalated beds of calc-silicates, carbonate-cemented bedded tuffs, and (locally fossiliferous) limestone in the Ritter Range pendant are a principal line of evidence for marine deposition of the Koip sequence. Huber and Rinehart (1965) suggested correlation of the Ritter Range pendant to compositionally similar volcanoclastic rocks in the western Mount Morrison pendant (Rinehart and Ross, 1964), though the precise connection between the two pendants is obscured by a cover of Neogene volcanic rocks associated with the Long Valley caldera.

In this study we sampled weakly deformed ignimbrite horizons with relatively well-preserved primary igneous textures from the volcanoclastic section in the Ritter Range pendant (Figures 2 and 3). Petrographically, tuffs throughout the eastern Ritter Range pendant are broadly similar, felsic lapilli tuffs, containing lithic fragments, flattened pumice lapilli, and relict phenocrysts in a finer-grained and recrystallized quartzofeldspathic matrix (Figure 5). Tuffs in the easternmost part of the section are porphyritic with 10 to 25% phenocrysts of quartz, feldspar, and pseudomorphs of biotite. Farther to the west, tuffs are commonly relatively crystal-rich, with 25-40% phenocrysts of quartz, feldspar, and pseudomorphs of biotite \pm amphibole. Quartz phenocrysts preserve igneous textures with subhedral to locally euhedral outlines that are deeply

embayed, despite pervasive deformation lamellae and subgrain development, and feldspar phenocryst are mostly subhedral although commonly fractured.

All early Mesozoic volcanoclastic rocks in the eastern Ritter Range pendant are vertical to steeply southwest dipping and upright, and are cut by shear zones at very low angles to compositional layering (Figure 3; Fiske and Tobisch, 1978; Tobisch et al., 1986; Bateman, 1992). Strain markers, primarily quartz phenocrysts and lapilli in tuffs and clasts in tuff breccias, suggest highly heterogeneous flattening strains, with average elongations of 30 to 50% measured perpendicular to foliation (Tobisch et al., 1977). All units have been metamorphosed in albite epidote hornfels to hornblende hornfels facies at temperatures of ~400° to 550°C and pressures less than 300 MPa (Hanson et al., 1993). In tuffs, cleavage development and metamorphism resulted in matrix recrystallization to quartz + feldspar + biotite + muscovite + chlorite. Pyroxene hornfels facies assemblages were developed <0.5 km from contacts with intrusive rocks of the Late Cretaceous Tuolumne Intrusive Suite (Hanson et al., 1993; Sorensen et al., 1998). This observation is consistent with 85 to 80 Ma hornblende and mica $^{40}\text{Ar}/^{39}\text{Ar}$ ages indicating Late Cretaceous metamorphism following regional tilting and faulting of the volcanic section (Tobisch et al., 2000; Sharp et al., 2000).

Fiske and Tobisch (1978) and Tobisch et al. (1977, 2000) used all available published and unpublished, conventional zircon bulk-fraction thermal ionization mass spectrometry (TIMS) ages to divide the metavolcanic section in the eastern Ritter Range pendant into four structural blocks (Figure 3). Block I was interpreted to contain Late Triassic to Early Jurassic volcanoclastic rocks overlain along an unconformity by a tuff dated at ~163 Ma and associated

tuff breccias and lavas. Block II was interpreted to contain a repeated sequence of upper Block I units, including proposed correlation of a tuff dated at two localities at 163 and 164 Ma with the 163 Ma tuff in Block I. An Early Jurassic age for at least part of Block II is supported by the presence of pelecypod *Weyla* in a limestone bed near the base of the block north of Garnet Lake (Rinehart et al., 1959). Block III was interpreted to contain an imbricated section of Late Triassic (211 and 203 Ma) tuffs and associated Late Triassic to Early Jurassic volcanoclastic rocks. Block IV was interpreted to contain Early to Middle Jurassic volcanoclastic rocks. In this study we report thirteen new ages from tuffs in Block I that support a general early Mesozoic age assignment but require a more complex structural evolution for the block, and three new ages from block II to test the correlation of tuffs with Block I.

ANALYTICAL METHODS

Isotopic compositions and minor and trace element abundances in zircon were measured by secondary ion mass spectrometry (SIMS) on the U.S. Geological Survey SHRIMP-RG ion microprobe at Stanford University. Grains were mounted in epoxy and polished to expose grain interiors, and imaged with a scanning electron microscope using a cathodoluminescence detector. Isotopic ratios and U, Th, and Pb concentrations were measured using a ~30 μm diameter, 4 nA O_2^- primary beam and data reduction procedures described in Barth and Wooden (2006). Measured ages were standardized to zircons from the Middledale Diorite (TEMORA-2, 416.8 Ma; Black et al., 2003, 2004) or the Braintree Complex (R33, 419 Ma; Black et al., 2004) (Table S1). Errors on individual spot ages are reported at 1 sigma, and weighted mean ages of populations of zircons are reported at the 2 sigma (95% confidence) level (Table 1). Following age determinations, grain mounts were lightly polished to remove sputtered pits, recoated with

gold, and analyzed for a suite of trace elements using a ~15 to 20 μm diameter, 1 to 2 nA O_2^- primary beam; analytical and data reduction procedures were described by Barth and Wooden (2010) (Table S2). $^{206}\text{Pb}/^{238}\text{U}$ was measured at the end of each trace element mass scan to assure that elemental data came from a zircon volume of the same age as determined from dated spots. Concentrations were standardized against Madagascar Green zircons (MAD, MADDER; Mazdab and Wooden, 2006).

Major elements in tuff whole rocks were measured by x-ray fluorescence and trace elements were measured by inductively coupled plasma–mass spectrometry at Michigan State University (Table S3). In-run precision was monitored using JB-1a and BHVO basalt standards, and is better than 1% for most major elements and trace elements present in abundances >100 ppm, and is typically 2-5% for less abundant trace elements. Additional whole rock major element analyses analyzed as part of the Sorensen et al. (1998) study are also reported in Table S3.

ZIRCON U-PB GEOCHRONOLOGY

SIMS geochronology of felsic tuffs in the Ritter Range is based on $^{206}\text{Pb}^*/^{238}\text{U}$ spot ages in single detrital grains, with radiogenic Pb ($^{206}\text{Pb}^*$) corrected for common Pb using measured $^{207}\text{Pb}/^{206}\text{Pb}$ (Ireland and Williams, 2003). Ages based on $^{207}\text{Pb}/^{235}\text{U}$ and $^{207}\text{Pb}/^{206}\text{Pb}$ are not reported due to large uncertainties in measured ^{207}Pb and calculated ratios. Most samples yielded a single dominant population (typically 70 – 90%) of grains in terms of measured $^{206}\text{Pb}^*/^{238}\text{U}$ ages, and calculated ages of tuffs are based on the weighted mean $^{206}\text{Pb}^*/^{238}\text{U}$ age of this population (Table 1). Less common younger grains are assumed to have experienced minor Pb loss during metamorphism and/or exhumation. Rare older grains may represent premagmatic

zircons or zircons from entrained lithic lapilli, although every effort was made to exclude lithic fragments during sample preparation for geochronologic analysis.

New SIMS ages significantly increase the database of zircon ages for volcanic rocks in the east central Sierra Nevada. $^{206}\text{Pb}^*/^{238}\text{U}$ ages indicate a strongly bimodal distribution of crystallization ages for Ritter Range tuffs (Figures 6 and 7), mostly in Late Triassic and Middle Jurassic time. The majority of the tuffs (14 of 16 samples) yield ages that fall within the Triassic or Middle to Late Jurassic magmatic pulses (p1, p2) of the California arc (Barth et al., 2013). Five Triassic samples also contain one or more distinctly older grains; the majority of these are 226 to 227 Ma (n=6), with a single grain at 235 Ma.

In order to determine stratigraphic and structural relations in Block I, the least understood part of the eastern Ritter Range pendant, we dated multiple samples of felsic tuffs in the upper San Joaquin River drainage (Figures 2 and 3). Tobisch et al. (2000) reported a 164 ± 2 Ma conventional TIMS bulk fraction zircon age for a quartz-rich ash flow tuff ('lower tuff unit' from the middle of Block I east of Garnet Lake. Tobisch et al. suggested that older units lay to the east in Block I, beneath this tuff and above Paleozoic metasedimentary rocks. Five tuff samples from the eastern part of this block yielded indistinguishable SIMS ages between 221 ± 2 and 218 ± 2 Ma. These samples include the tuffs of San Joaquin Mountain and Agnew Meadows, the lowermost tuff units preserved unconformably above Paleozoic metasedimentary rocks. In contrast, tuffs exposed higher in the sequence along the San Joaquin River (tuffs of Olaine Lake and lower Shadow Falls) yield well-defined Middle Jurassic ages of 171 ± 2 and 168 ± 2 Ma (Figures 3 and 4). West of the river and still higher in the sequence, four thin tuff units yielded

Late Triassic ages, two at 219 Ma that overlap in age with the tuffs of Agnew Meadows and San Joaquin Mountain, and two that are significantly younger, with ages of 206 and 207 Ma. The prominent thick tuff units exposed between Rosalie Lake and Garnet Lake yielded well-defined Jurassic ages of 169 ± 2 to 167 ± 2 Ma. In sum, SIMS ages do not yield a spatial pattern of ages consistent with an upright west-facing sequence in Block 1 (Figures 3 and 4). Rather, the data are consistent with a repeated succession of Triassic and Jurassic units indicative of a structural stratigraphy in Block I that includes at least three imbricated sequences of early Mesozoic volcanoclastic rocks.

We dated three samples of felsic tuffs from Block II in order to determine stratigraphic relations within this block and to test proposed correlation with tuff units in Block I (Figure 3). Tobisch et al. (2000) reported a 164 ± 2 Ma conventional TIMS zircon age for a quartz-rich ash flow tuff ('upper tuff unit' from the base of Block II that crops out in lower Shadow Meadows and an age of 163 ± 2 for a sample from the same tuff unit near Garnet Lake. Our sample of the tuff of lower Shadow Meadows yielded an age of 170.8 ± 1 Ma, and a second sample of a thinner tuff slightly higher in the section yielded a slightly younger age of 168.6 ± 1 Ma. The SIMS age of the tuff of lower Shadow Meadows is older than the conventional TIMS age reported by Tobisch et al. (2000). However, the SIMS ages of the tuffs of upper and lower Shadow Meadows do provide support for their proposed correlation with the 'lower tuff unit' in Block I, which yielded a SIMS age of 169 ± 2 Ma. Higher in the section within Block II, a thin tuff near Garnet Lake yielded a Jurassic age of 174 ± 3 Ma; the age of this sample is less precise as it is more strongly affected by loss of radiogenic Pb than is typical for Jurassic samples in this study.

Felsic volcanic rocks in the Mount Morrison pendant lie along strike with the volcanic sequences in Block I in the Ritter Range pendant, the connection obscured beneath the cover of the Neogene Mammoth Mountain volcanic complex, and were tentatively correlated with them by Huber and Rinehart (1965; Figure 1). In the Mount Morrison pendant, the most prominent marker unit is the ~1.2 km thick, porphyritic rhyolite tuff of Skelton Lake. A sample of the tuff collected near Duck Pass yielded an age of 216.5 ± 1 Ma, overlapping in age with the texturally and compositionally similar rhyolitic upper tuff of San Joaquin Mountain (Table 1).

WHOLE ROCK GEOCHEMISTRY

Classification of the Ritter Range ignimbrites is based on phenocryst abundances and major element contents of whole rocks. Quartz and feldspar phenocryst abundances range from 10 to 40%, and silica contents range from 66 to 76% (Figure 8), suggesting classification of the tuffs as arc-type, phenocryst-rich dacites and rhyolites. The lowest overall silica content was found in the Jurassic phenocryst-rich dacite tuff of west Shadow Lake. Most other tuffs are broadly similar to low-silica rhyolite tuffs, with a few samples from several of the tuffs ranging to high-silica rhyolite.

Although silica contents largely overlap between the two age groups, alkali contents are distinctive. Contents of K_2O are distinctly high in most Jurassic tuffs, ranging from 5.5 to over 10%, higher values than observed in modern arc-type ash-flow tuffs. High K_2O contents in Jurassic tuffs are also associated with low Na_2O and Sr contents (Figure 9). Hanson et al. (1993) and Sorensen et al. (1998) showed that these high K_2O contents are associated with metasomatic mineral assemblages and high $\delta^{18}O$ values, concluding that much of the observed K enrichment

and Na and Sr depletion resulted from seawater alteration at low temperatures soon after deposition. In contrast, the Jurassic dacite tuff of west Shadow Lake and all Triassic tuffs do not have comparably high whole rock alkali contents that would be indicative of potassic metasomatism.

Fluid-immobile high field strength element abundances support classification of the ignimbrites as arc-type dacite and low silica rhyolites and provide additional insight into possible secular variations (Figures 8 and 9). Titania and Al_2O_3 abundances indicate the major element compositional similarity of Triassic and Jurassic samples. Rare earth element (REE) abundances are also broadly similar; however, Jurassic tuff whole rock samples are generally enriched in Th, Zr, and light rare earth elements (REE). This latter observation suggests that some of the differences in lithophile element abundances between tuffs may reflect relative lithophile element enrichment of Jurassic silicic magmas.

ZIRCON GEOCHEMISTRY

Zircons from proximal arc volcanoclastic rocks complement whole rock geochemical data indicative of tectonic setting and evolution of silicic melts, because of the resistance of zircon to recrystallization during hydrothermal alteration and low-grade metamorphism. Hafnium and trace element analyses of magmatic zircons provide independent estimates of the compositional characteristics and evolution of Triassic and Jurassic silicic melts following zircon saturation. Zircons in the Ritter Ranges tuffs are compositionally variable, both within and between grains within a given rock sample, primarily reflecting both varying crystal growth histories and progressive silicic melt fractionation following zircon saturation. Grimes et al. (2015) and Barth

et al. (2017) have established that zircon compositional ranges reflect specific tectono-magmatic environments. The zircon compositional data from the Ritter Range, combined with data from Saddlebag Lake pendant (Barth et al., 2012), not only provide information about melt evolution but also confirm the compositionally distinct nature of Jurassic melts, consistent with the differences in the whole rock major and trace element data presented above.

It is well established that zircon changes systematically toward higher Hf and lower Ti when crystallizing in a melt with evolving composition and falling temperature (e.g. Anderson et al., 2008; Claiborne et al., 2010). Overall ranges in Hf and Ti abundances may reflect in part differences in initial melt compositions upon saturation, and changes in Hf and Ti contents within samples result from bulk fractionation of the melt and the sensitivity of zircon/melt partition coefficients to changing temperature. Hafnium contents in Ritter Range magmatic zircons range from 7,000 to 14,000 ppm. Overlapping Hf abundances in Triassic and Jurassic suites indicate similar ranges of melt fractionation, consistent with the broad similarity in whole rock compositions of the tuffs. Titanium abundances are negatively correlated with Hf in most individual samples and in suites, and differences in the range of Ti abundances in the main compositional groups suggest that zircon growth in the Triassic melts occurred at relatively lower temperatures (Figure 10). Although Ti concentrations in early, low Hf zircons are similar for the Triassic and Jurassic main groups, at 9,000 - 11,000 ppm Hf (relatively nearer the solidus), Ti concentrations in Triassic zircons range from 2-6 ppm, compared to 5-10 ppm in Jurassic zircons. This difference indicates that in the later stage of melt evolution the Triassic melts either had a lower a_{TiO_2} or were $\sim 50^\circ\text{C}$ cooler than the most common Jurassic melts.

Titanium concentrations for the relatively young (207 Ma) Triassic sample fit best with the Jurassic main group, a pattern that is repeated for several other compositional characteristics.

Ritter Range zircons are divided into four groups based on age and composition. The zircons from most Triassic tuffs define a main, coherent group for most element abundances and ratios, such as Hf and Ce/U (Figure 10), and zircons from Saddlebag Lake tuffs of similar age are compositionally part of this main group. However, zircons from the two relatively young (206 and 207 Ma) Triassic tuffs in the Ritter Range often separate from this main Triassic group, with compositions intermediate between the main Triassic and Jurassic compositional groups. The Jurassic data define two compositional groups of the same age. The main Jurassic population is distinct in many compositional characteristics from Triassic zircons, especially in higher Ti and Ce/U. In contrast, zircons in two Jurassic tuffs (lower Shadow Falls, Olaine Lake) are compositionally similar to Triassic data, and zircons in the dacite tuff of west Shadow Lake are mixed, with zircons overlapping both the Triassic and Jurassic main compositional groups. The age range for the Jurassic samples is limited and the individual ages are not precise enough to determine if the compositional differences within the Jurassic group are related to small differences in age, as they are for the older and younger Triassic zircons.

Compositional differences between the main Triassic and Jurassic zircon groups, and the transitional character of the relatively young Triassic tuffs, are reinforced by variations in normalized U, Ce, and Th abundances (Figure 11). The Triassic zircons, including those in the younger samples, are characterized by Th/U of ~0.2 to 0.5, while the main Jurassic zircon group typically has significantly higher Th/U ~0.5 to 1.4 and as high as ~2. Although U concentrations

are largely overlapping, average U for the older Triassic is about twice that of the Jurassic (~1,000 vs. 500 ppm), and the younger Triassic zircons are distinct with U mostly less than 300 ppm. Ce/Yb increases with U/Yb and Hf concentrations in magmatic zircons. The main group of Jurassic zircons record growth in melts with higher Ce/Yb and Th/U relative to Hf and U/Yb. These observations are consistent with the relative LREE and Th enrichments observed in Jurassic tuff whole rocks.

In summary the main Ritter Range Triassic and Jurassic zircon compositional groups are distinct from each other in several key trace element compositional characteristics, including U/Yb (higher in the Triassic), and Ce/U, Ce/Yb, and Th/U (all higher in the Jurassic). The data for the two young Triassic samples are distinct from the main older Triassic group and in some characteristics appear transitional to the main Jurassic group. Two of the Jurassic tuffs have zircon compositions very similar to those of the main Triassic group and zircons from a third Jurassic tuff have mixed compositions. As will be discussed below, the striking differences in Triassic and Jurassic zircon compositions indicate that silicic magma sources and/or fractionation processes changed systematically from the Triassic to Jurassic, where distinct and more diverse silicic melts were produced in Jurassic time.

DISCUSSION

The Triassic to Jurassic volcanoclastic rock sequence of the Ritter Range pendant constitutes a record of inception and early evolution of the Sierran volcanic arc. Petrologic data are relatively limited for this early arc stage, in comparison to the voluminous mid- to Late Cretaceous episode of arc magmatism. Populations of magmatic zircons from this study provide ages for multiple

ignimbrite marker units from the eastern part of the pendant, in particular improving the temporal resolution in the oldest volcanoclastic rocks along and east of the San Joaquin River. Zircon trace element data reinforce the arc affinity of the ignimbrites and provide further understanding of the chemical evolution of early arc silicic melts. Below we discuss how zircon ages illuminate regional correlations between early arc volcanic sections, and how ages and compositions of zircons constrain arc inception and record the secular changes in silicic melts in the evolving arc.

Regional Extent of Tuffs - - Sierran Volcanic Arc Inception and Growth

The northwest-trending Cordilleran orogen is inferred to have been established by initiation of convergence along a sinistral transform boundary that truncated the pre-existing craton margin (Burchfiel and Davis, 1981; Stone and Stevens, 1988; Burchfiel et al., 1992; Dickinson, 2008; Saleeby, 2011). In the central Sierra Nevada region, initiation of convergence along the transform zone is marked by mélangé formation and high-pressure metamorphism in the western Foothills Terrane. There, the best estimate of the timing of subduction initiation comes from the 255 ± 20 Ma age of a garnet amphibolite block in the Kaweah mélangé, where the mélangé is nonconformably overlain by ~219 Ma tholeiitic to boninitic lavas that may record supra-subduction zone infant arc magmatism (Saleeby, 2011).

Precise geochronologic data for early Sierran arc volcanic successions are another key to constraining subduction inception, through timing the initiation of volcanism and style of silicic arc magmatism along the pre-existing transform margin. In the east central Sierra Nevada, deposition of volcanoclastic rocks above deformed Paleozoic metasedimentary rocks provides a

record of the inception of arc volcanism (Kistler, 1966; Bateman, 1992; Saleeby and Busby, 1993; Schweickert and Lahren, 1993, 2006; Barth et al., 2011). SIMS ages and field relations in the Ritter Range pendant, when linked to correlative stratigraphic sections to the north and south in Saddlebag Lake and Mount Morrison pendants, respectively, provide a broad regional record of initiation of the juvenile Sierra Nevada volcanic arc. Ages of ignimbrites are compared to each other and to ages of plutonic whole rocks from underlying intrusive suites in Figure 7. The 221 to 216 Ma tuffs in the eastern Ritter Range are coeval with Late Triassic tuffs in the Saddlebag Lake pendant and southward into the Mount Morrison pendant. The oldest ash flow-tuff in Saddlebag Lake pendant extends the Triassic volcanic record back to 232 Ma. Volcanic arc inception no later than Early to early Late Triassic time in this region is supported by the oldest individual grains dated from these Triassic tuffs, as old as 235-236 Ma in both the Saddlebag Lake and Ritter Range pendants. Granodioritic to granitic rocks of the underlying Scheelite Intrusive Suite range in age from 226 to 218 Ma, indicating that batholith construction began within about 10 m.y. of the beginning of juvenile arc silicic volcanism.

Consideration of the regional magmatic record suggests that arc inception and the first pulse of magmatism in Triassic time was followed by a magmatic lull in the east Sierran arc, reflected in both the volcanic record and the ages of plutons in the underlying batholith. This lull, a period from about 215 to 175 Ma of persistent low-volume magmatism, is marked in the Ritter Range pendant by tuff breccias, mafic lava flows, and rare thin silicic tuffs dated at ~211 to 203 Ma. The magmatic lull was followed by rejuvenation of voluminous silicic magmatic arc activity in late Early Jurassic time. Existing data show that both plutons and ignimbrites record this second pulse of magmatic activity (e.g., Figure 7). Ages of Jurassic tuffs in the eastern Ritter Range

pendant range from 174 to 167 Ma, extending to Middle Jurassic ages as young as measured in the Oak Creek pendant further south in the eastern Sierra Nevada and coeval with underlying quartz dioritic to granitic batholithic rocks of the Palisade Crest Intrusive Suite. Ignimbrites in the Saddlebag Lake, Ritter Range and Mount Morrison pendants, petrographically similar to modern “monotonous intermediate” dacite or phenocryst-poor low-silica rhyolite, are therefore regionally spatially associated and coeval with underlying granodioritic to granitic components of the early Mesozoic Sierra Nevada batholith. The accumulating evidence of zircon age data thus suggests that explosive silicic volcanism in the Sierra Nevada volcanic arc and pulses of felsic plutonism in the underlying batholith were closely coupled at one- to two-million-year time scales, from mid-Triassic arc inception through Middle Jurassic time.

Silicic Melt Compositional Diversity in the Early Sierran Volcanic Arc

Trace element analyses of zircons from global data sets indicate a continuum of compositions over a range of tectonomagmatic settings: (1) mid-ocean ridges through back-arc to oceanic intra-plate settings, (2) oceanic to continental arc settings, and (3) rifts and plumes in continental lithosphere (Claiborne et al., 2010; Grimes et al., 2015; Barth et al., 2017). Zircons from mid-ocean ridge (Mid-Atlantic and southwest Indian ridges), back-arc (Parece Vela) and oceanic intraplate (Iceland) settings establish the range of trace element patterns in zircons from magmatic systems not influenced by subduction (Grimes et al., 2009; Carley et al., 2011). In comparison to these tectonomagmatic settings, zircons from convergent-margin arcs show characteristic depletion in Nb, an element conserved in the slab, and enrichment in U and Th, reflective of slab contributions to arc magmas (e.g. Pearce, 1982). Arc zircons are also

characterized by high Sc/Yb, which is related to high water contents and lack of extensive basalt fractionation in arc parent melts prior to zircon saturation (Grimes et al., 2015).

Zircons from both the eastern Sierra Triassic and Jurassic magmatic suites exhibit trace element compositions consistent with those expected for convergent margin settings, including high Sc/Yb relative to U/Yb (Figure 12), decreasing Sc/Yb with increasing U/Yb, with a small fraction of the samples overlapping the compositional range of intra-plate zircons. The compositions of Izu-Bonin arc zircons are shown for reference, emphasizing the similarity in Sc but significantly higher U/Yb in both the Sierran suites, especially the Triassic, compared to this modern, primitive oceanic arc.

Zircons with U/Yb greater than ~0.1-0.2 (and Th/Yb greater than ~0.1) characterize continental arc magmatic suites and provide the foundation for the success of U/Yb and Nb/Yb in distinguishing zircons from the depleted MORB and primitive oceanic arc environments from the more enriched U and Th continental arc zircons (Grimes et al., 2015; Barth et al., 2017; Figure 13). Oceanic arc zircons are transitional in composition between the mid-ocean ridge and continental arc data arrays. A useful approach to differentiate among arc zircon suites is based on their level of U/Yb enrichment, which extends from the lowest in oceanic arcs such as the Aleutians and Izu-Bonin (U/Yb as low as 0.04 but extending to 0.1-0.3) to moderately enriched suites with U/Yb ~0.1 to 1 (Cascades), to strongly enriched suites with U/Yb ≥ 1 (Andes, Sierra Triassic). In general U/Yb ranges in zircon suites follow the major element characteristics of their host melts. Zircons from the early Izu-Bonin arc, a relatively lithophile element-depleted (low to medium K) juvenile oceanic arc, record growth in less enriched, low U/Yb silicic melts

compared to medium and high U/Yb melts from relatively lithophile element-enriched (medium to high K) transitional and continental settings such as the Cascade and Andean arcs.

Triassic and Jurassic zircons in the Ritter Range pendant have medium to high U/Yb and Nb/Yb ~0.01 to 0.05, similar to those in modern medium to high K arcs. Triassic and Jurassic zircons are enriched in Nb as well as U compared to zircons from mid-ocean ridges and Izu-Bonin oceanic arc zircons, likely reflecting relative contributions of both slab and lithospheric mantle to enriched melt compositions in the Sierran arc. Older Triassic zircons have uniformly high U/Yb, overlapping with zircons from contemporaneous volcanoclastic rocks from the Saddlebag Lake and Mount Morrison pendants and 2 to 3 times higher than typical Jurassic zircons over similar ranges in Hf concentrations. These data indicate that Triassic zircons across a significant strike length of the juvenile Sierran arc record early arc silicic melts that were significantly U-enriched compared to silicic melts in the juvenile Izu-Bonin arc, and significantly enriched relative to melts formed later in the evolving arc in Jurassic time.

The strong U enrichment in Triassic zircons is also reflected in very low Th/U. The Triassic zircons have Th/U mostly ~0.2-0.5, among the lowest ranges observed for arc magmatic suites, which typically have a Th/U range of 0.5-1.0. Although enrichment of U and Th is a hallmark of arc magmatism, it appears that extreme U enrichment is not accompanied by comparable Th enrichment in this case. The east Sierra Jurassic zircons have significantly higher Th/U, mostly 0.5 to 1.5, ranging up to 2.1 and extending to values higher than is typical of arc magmatic suites. If relative U and Th abundances are controlled by slab fluid characteristics, then the nature of the slab contribution was dramatically different between the Triassic and Jurassic,

possibly because of more water-rich, oxidizing conditions in the Triassic. Alternatively, the observed differences might be the result of differences in lithospheric source composition.

Jurassic zircons formed after a significant regional lull in Sierran volcanism between about 216 and 174 Ma. Zircons in Jurassic rocks show significant differences in average composition relative to Triassic zircons from the juvenile arc. The high Ti, high Th/U and relatively low U/Yb in Jurassic zircons can be explained by formation of relatively hotter melts and by partial decoupling of U from Th in the Jurassic volcanic arc. Relative Ce abundances are also very different between the main east Sierra Triassic and Jurassic zircon groups with the Jurassic having a much stronger Ce enrichment. Decoupling of U from Th and Ce could reflect the relative temperature of the slab-derived component, with relatively higher-T fluid or slab melt playing a more important role in Jurassic volcanism. Alternatively, hydrous melting of a relatively enriched lithospheric mantle and/or lower crustal source of southwestern US (Mojave) craton-type could have been a more important component of magmatism in the Jurassic arc, reflecting rearrangement of the sub-arc lithosphere (shortening?) as the arc evolved.

Structural Stratigraphy of the Ritter Range Pendant

Based on conventional TIMS zircon ages, Tobisch et al. (2000) divided the volcanic section in the Ritter Range pendant into four structural blocks (Figure 3) and reasoned that the section is duplicated by cryptic thrust faults subparallel to bedding. New SIMS ages for ignimbrites reported here expand on this model for the local and regional tectonic stratigraphy of Mesozoic metavolcanic rocks in the pendant (Figures 3 and 4). Zircon ages of 169 to 171 Ma for the tuffs of Rosalie Lake and lower Shadow Meadows (lower and upper tuff units) are older than TIMS

ages, but within uncertainties allow correlation of these tuffs, as suggested by Tobisch et al. (2000) and supported by similar whole rock compositional ranges (Figure 8). However, both Triassic and Jurassic tuffs are exposed beneath the tuff of Rosalie Lake and the 167 Ma tuff of West Shadow Lake lies above it, indicating that blocks I and II both contain repeated stratigraphic sections. Tobisch et al. (2000) previously proposed a similar history of internal imbrication for block III as well. Thus, geochronologic data indicate that most or all of the early Mesozoic section in the eastern Ritter Range pendant is an internally imbricated composite volcanic section.

Tobisch et al. (2000) suggested that tilting and imbrication of the volcanic section primarily records northeast-directed thrusting between 164 and 105 Ma. Fabrics along exposed, faulted contacts between imbricated blocks consistently show steeply plunging lineations and a predominant component of west-side-up shear (Tobisch and Fiske, 1982; Sharp et al., 2000). Metavolcanic rocks with comparable steep dips extend to the north into the Saddlebag Lake pendant, where they were interpreted to have been imbricated by thrusting in Late Jurassic time (Schweickert and Lahren, 2006; Barth et al., 2011). To the south, comparably steeply dipping Middle Jurassic metavolcanic rocks in the Oak Creek pendant were deformed and tilted prior to emplacement of the Independence dike swarm (Saleeby et al., 1990; Barth et al., 2014). Regional continuity in the style and timing of Late Jurassic imbrication and tilting of the early Mesozoic arc section in the eastern Sierra thus is likely to record the development of the East Sierran thrust system (Tobisch et al., 2000; Schweickert and Lahren, 1993, 2006; Dunne and Walker, 2004). Steeply dipping ductile fabrics with subhorizontal stretching lineations along the contact between the metavolcanic section and Paleozoic metasedimentary rocks record later dextral shear linking

the Cretaceous Gem Lake and Rosy Finch shear zones (Greene and Schweickert, 1995; Tikoff and Saint Blanquat, 1997; Tikoff and Greene, 1997). Overall regional tilting may have been enhanced by later downward flow during pluton emplacement in the Cretaceous arc (Tobisch et al., 2000).

CONCLUSIONS

Although ignimbrites in the Ritter Range pendant exhibit a wide range of SIMS U-Pb ages, regional correlations across several pendants suggest first-order episodic production of zircon-saturated silicic melts in the juvenile Sierran volcanic arc. Distinct pulses of ignimbrite deposition at ca. 221 to 216 Ma and 174 to 167 Ma were coeval with plutons of the underlying batholith, indicating that explosive silicic arc volcanism and batholith construction were closely coupled at relatively short time scales. The geochemistry of zircons records secular variation in silicic melts in the volcanic arc, suggesting significant changes in the nature of the slab contributions and/or overriding plate lithospheric magma sources between the juvenile Triassic and mature Jurassic arc stages. Future geochronologic and Hf and Pb isotopic studies in well-dated volcanoclastic arc sections can clarify the nature of the diminished arc magmatic flux between these two pulses of ignimbrite deposition, and the pace and style of changes in mafic and silicic lithospheric magma sources as the arc evolved.

ACKNOWLEDGMENTS

Support for this research was provided by the U.S. National Science Foundation through grants EAR-1348059 and OCE-1558830, and by the IUPUI Research Support Fund. M. Coble provided critical and timely assistance with SIMS analyses. We thank R. Fiske and B. Hanson for

generously sharing their observations and insights about the Ritter Range. We appreciate discussions about the Koip sequence with D. Greene, R. Kistler, and R. Schweickert, and discussions about arc zircon data with T. Carley, D. Clemens-Knott, J. Gill, C. Grimes, and K. Surpless. This manuscript benefited from reviews by E. Todd and an anonymous reviewer.

Supporting data are included as supplementary data files.

REFERENCES

- Anderson, J.L., Barth, A.P., Wooden, J.L., and Mazdab, F., 2008, Thermometers and thermobarometers in granitic systems, in Putirka, K.D., and Tepley, F.J., eds., *Minerals, Inclusions and Volcanic Processes: Mineralogical Society of America Reviews in Mineralogy*, 69, 121-142.
- Aramaki, S., 1984, Formation of Aira caldera, southern Kyushu, 22,000 years ago: *Journal of Geophysical Research*, 89, 8485-8501.
- Arculus, R.J., Ishizuka, O., Bogus, K.A., Gurnis, M.C., Hickey-Vargas, R., Aljehdali, M.H., Bandini, A.N., Barth, A.P., Brandl, P.A., Drab, L., Guerra, R., Hamada, M., Jiang, F., Kanayama, K., Kender, S., Kusano, Y., Li, H., Loudin, L.C., Maffione, M., Marsaglia, K.M., McCarthy, A., Meffre, S., Morris, A., Neuhaus, M., Savov, I.P., Sena, C., Tepley, F.J., van der Land, C., Yogodzinski, G.M., and Zhang, Z., 2015a, A record of spontaneous subduction initiation in the Izu-Bonin-Mariana arc: *Nat. Geosci.*, 8, 728-733, doi: 10.1038/ngeo2515.

Barth, A.P., and Wooden, J.L., 2006, Timing of magmatism following initial convergence at a passive margin, southwestern U.S. Cordillera, and ages of lower crustal magma sources:

Journal of Geology, 114, 231-245, doi: 10.1086/499573.

Barth, A.P., and Wooden, J.L., 2010, Coupled elemental and isotopic analyses of polygenetic zircons from granitic rocks by ion microprobe, with implications for melt evolution and the sources of granitic magmas: *Chemical Geology*, 277, 149-159.

Barth, A.P., Walker, J.D., Wooden, J.L., Riggs, N.R. and Schweickert, R.A., 2011, Birth of the Sierra Nevada magmatic arc: Early Mesozoic plutonism and volcanism in the east-central Sierra Nevada of California: *Geosphere*, 7, 877-897.

Barth, A.P., Feilen, A.D.G., Yager, S.L., Douglas, S.R., Wooden, J.L., Riggs, N.R., and Walker, J.D., 2012, Petrogenetic connections between ash-flow tuffs and a granodioritic to granitic intrusive suite in the Sierra Nevada arc, California: *Geosphere*, 8, 250-264, doi:10.1130/GES00737.1.

Barth, A.P., Wooden, J.L., Jacobson, C.E., and Economos, R.C., 2013, Detrital zircon as a proxy for tracking the magmatic arc system: the California arc example: *Geology* 41, 223-226, doi:10.1130/G33619.1.

Barth, A.P., Riggs, N.R., Walker, J.D., Andrew, J.E., Jacobson, C.E., Miller, D.M., and Robert, J., 2014, Petrogenetic connections between volcanic rocks and intrusive suites in the California arc - toward an integrated model for upper-crustal magma system evolution: *EOS Transactions AGU 95*, Fall Meeting Supplement V33B-4849.

Barth, A.P., Tani, K., Meffre, S., Wooden, J.L., Coble, M.A., Arculus, R.J., Ishizuka, O., and Shukle, J.T., 2017, Generation of silicic melts in the early Izu-Bonin arc recorded by detrital

zircons in proximal arc volcanoclastic rocks from the Philippine Sea: *Geochemistry, Geophysics, Geosystems*, 18, doi: 10.1002/2017GC006948.

Bateman, P.C., 1992, Plutonism in the central part of the Sierra Nevada batholith, California: U.S. Geological Survey Professional Paper 1483, 186 pp.

Bateman, P.C., Kistler, R.W., Peck, D.L., and Busacca, A.J., 1983, Geologic map of the Tuolumne Meadows Quadrangle, Yosemite National Park, California: U.S. Geological Survey Map GQ-1570, scale 1:62,500.

Black, L.P., Kamo, S.L., Allen, C.M., Aleinikoff, J.N., Davis, D.W., Korsch, R.J. and Foudoulis, C., 2003, TEMORA 1: a new zircon standard for Phanerozoic U–Pb geochronology: *Chemical Geology*, 200, 155-170.

Black, L.P., Kamo, S.L., Allen, C.M., Davis, D.W., Aleinikoff, J.N., Valley, J.W., Mundil, R.M., Campbell, I.H., Korsch, R.J., Williams, I.S., and Foudoulis, C., 2004, Improved $^{206}\text{Pb}/^{238}\text{U}$ microprobe geochronology by the monitoring of a trace-element-related matrix effect: SHRIMP, ID-TIMS, ELA-ICP-MS, and oxygen isotope documentation for a series of zircon standards: *Chemical Geology*, 205, 115-140.

Brandl, P.A., Hamada, M., Arculus, R.J., Johnson, K., Marsaglia, K.M., Savov, I.P., Ishizuka, O., and Li, H., 2017, The arc arises: The links between volcanic output, arc evolution and melt composition: *Earth Planet. Sci. Lett.*, 461, 73-84, 10.1016/j.epsl.2016.12.027.

Burchfiel, B.C., and Davis, G.A., 1981, Mojave Desert and environs, in Ernst, W.G. (ed.), *The Geotectonic Development of California*: Englewood Cliffs, NJ, Prentice-Hall, 217-252.

Burchfiel, B.C., Cowan, D.S., and Davis, G.A., 1992, Tectonic overview of the Cordilleran orogen in the western United States, in Burchfiel, B.C., Lipman, P.W., and Zoback, M.L.

- (eds.), The Cordilleran Orogen: Conterminous U.S. (Geology of North America, Vol. G-3): Boulder, CO, Geol. Soc. Am., 407-479.
- Busby-Spera, C.J., 1984, Large-volume rhyolite ash flow eruptions and submarine caldera collapse in the lower Mesozoic Sierra Nevada, California: *Journal of Geophysical Research*, 89, 8417-8427.
- Carley, T.L., Miller, C.F., Wooden, J.L., Bindeman, I.N. and Barth, A.P., 2011, Zircon from historic eruptions in Iceland: reconstructing storage and evolution of silicic magmas: *Mineralogy and Petrology*, 102, 135-161.
- Chen, J.H., and Moore, J.G., 1982, Uranium-lead isotopic ages from the Sierra Nevada batholith, California: *Journal of Geophysical Research*, 87, 4761-4784.
- Claiborne, L.L., 2011, Understanding upper crustal silicic magmatic systems using the temporal, compositional and thermal record in zircon [Ph.D. Dissertation]: Nashville, Vanderbilt University, 375 pp.
- Claiborne, L.L., Miller, C.F., and Wooden, J.L., 2010, Trace element composition of igneous zircon: A thermal and compositional record of the accumulation and evolution of a large silicic batholith, Spirit Mountain, Nevada: *Contributions to Mineralogy and Petrology*, 160, 511-531.
- Coombs, M.L., and Vazquez, J.A., 2014, Cogenetic late Pleistocene rhyolite and cumulate diorites from Augustine Volcano revealed by SIMS ^{238}U - ^{230}Th dating of zircon, and implications for silicic magma generation by extraction from mush: *Geochemistry, Geophysics, Geosystems*, 15, 4846-4865.

- Crowder, D.F., Robinson, P.T., and Harris, D.L., 1972, Geologic map of the Benton Quadrangle, Mono County, California and Esmeralda and Mineral Counties, Nevada: U.S. Geological Survey Map GQ1013, scale 1:62,500.
- Dickinson, W.R., 2008, Accretionary Mesozoic–Cenozoic expansion of the Cordilleran continental margin in California and adjacent Oregon: *Geosphere*, 4, 329-353.
- Dilles, J.H., Kent, A.J., Wooden, J.L., Tosdal, R.M., Koleszar, A., Lee, R.G. and Farmer, L.P., 2015, Zircon compositional evidence for sulfur-degassing from ore-forming arc magmas: *Economic Geology*, 110, 241-251.
- Douglas, S.R., Riggs, N.R., Barth, A.P., and Economos, R.C., 2011, The breccia of Frog Lakes: Record of mafic arc magmatism in the Mesozoic Sierra Nevada, California: EOS Transactions AGU 92, Fall Meeting Supplement V21C-2506.
- Dunne, G.C., and Walker, J.D., 2004, Structure and evolution of the East Sierran thrust system, east central California: *Tectonics*, 23, TC4012, 23 p., doi:10.1029/2002TC001478.
- Field, D., Riggs, N.R., and Barth, A.P., 2017, Episodic Sierran arc magmatism expressed in volcanic strata of the Mount Morrison pendant, east-central Sierra Nevada, California: *GSA Abstracts with Programs*, 49, 7.
- Fiske, R.S., and Tobisch, O.T., 1978, Paleogeographic significance of volcanic rocks of the Ritter Range Pendant, central Sierra Nevada, California, in Howell, D.G., and McDougall, K.A., eds., *Mesozoic Paleogeography of the Western United States, Pacific Coast Paleogeography Symposium 2: Society of Economic Paleontologists and Mineralogists, Pacific Section*, 209-221.

- Fiske, R.S., and Tobisch, O.T., 1994, Middle Cretaceous ash flow tuff and caldera-collapse deposit in the Minarets Caldera, east-central Sierra Nevada, California: Geological Society of America Bulletin, 106, 582-593.
- Fiske, R.S., Naka, J., Iizasa, K., Yuasa, M., and Klaus, A., 2001, Submarine silicic caldera at the front of the Izu-Bonin arc, Japan: Voluminous seafloor eruptions of rhyolite pumice: Geological Society of America Bulletin, 113, 813–824.
- Gill, J.B., Hiscott, R.N., and Vidal, P., 1994, Turbidite geochemistry and evolution of the Izu-Bonin arc and continents: Lithos, 33, 135-168.
- Glazner, A.F., 1991, Plutonism, oblique subduction, and continental growth: An example from the Mesozoic of California: Geology, 19, 784-786.
- Greene, D.C., and Schweickert, R.A., 1995, The Gem Lake shear zone: Cretaceous dextral transpression in the northern Ritter Range pendant, eastern Sierra Nevada, California: Tectonics, 14, 945-961.
- Grimes, C.B., John, B.E., Cheadle, M.J., Mazdab, F.K., Wooden, J.L., Swapp, S. and Schwartz, J.J., 2009, On the occurrence, trace element geochemistry, and crystallization history of zircon from in situ ocean lithosphere: Contributions to Mineralogy and Petrology, 158, 757-783.
- Grimes, C.B., Wooden, J.L., Cheadle, M.J., and John, B.E., 2015, “Fingerprinting” tectono-magmatic provenance using trace elements in igneous zircon: Contributions to Mineral and Petrology, 170, 46.
- Hanson, R.B., Sorensen, S.S., Barton, M.D., and Fiske R.S., 1993, Long-term evolution of fluid-rock interactions in magmatic arcs: Evidence from the Ritter Range Pendant, Sierra Nevada, California, and numerical modeling: Journal of Petrology, 34, 23-64.

Huber, N.K., and Rinehart, C.D., 1965, Geologic map of the Devils Postpile Quadrangle, Sierra Nevada, California: U.S. Geological Survey Map GQ437, scale 1:62,500.

Ireland, T.R. and Williams, I.S., 2003. Considerations in zircon geochronology by SIMS: Reviews in Mineralogy and Geochemistry, 53, 215-241.

Ishizuka, O., Taylor, R.N., Yuasa, M., and Ohara, Y., 2011, Making and breaking an island arc: a new perspective from the Oligocene Kyushu-Palau arc, Philippine Sea: Geochemistry, Geophysics, Geosystems, 12, doi: 10.1029/2010GC003440.

Kistler, R.W., 1966a, Geologic map of the Mono Craters Quadrangle, Mono and Tuolumne Counties, California: U.S. Geological Survey Map GQ462, scale 1:62,500.

Kistler, R.W., 1966b, Structure and metamorphism in the Mono Craters Quadrangle, Sierra Nevada, California: U.S. Geological Survey Bulletin 1221-E.

Kistler, R.W., and Swanson, S.E., 1981, Petrology and geochronology of metamorphosed volcanic rocks and a middle Cretaceous volcanic neck in the east-central Sierra Nevada, California: Journal of Geophysical Research, 86, 10489-10501.

Krauskopf, K.B., and Bateman, P.C., 1977, Geologic map of the Glass Mountain Quadrangle, Mono County, California and Mineral County, Nevada: U.S. Geological Survey Map GQ1099, scale 1:62,500.

Lloyd, E. F., Nathan, S., Smith, I.E.M., and Stewart, R.B., 1996, Volcanic history of Macauley Island, Kermadec Ridge, New Zealand: New Zealand Journal of Geology and Geophysics, 39, 295-308.

Mahan, K.H., Bartley, J.M., Coleman, D.S., Glazner, A.F. and Carl, B.S., 2003, Sheeted intrusion of the synkinematic McDoogle pluton, Sierra Nevada, California: Geological Society of America Bulletin, 115, 1570-1582.

Mazdab, F.K., and Wooden, J.L., 2006, Trace element analysis in zircon by ion microprobe (SHRIMP-RG): technique and applications: *Geochimica et Cosmochimica Acta*, 70(S1), A405.

McDonough, W.F. and Sun, S.-S., 1995, Composition of the Earth: *Chemical Geology*, 120, 223-253.

Pearce, J.A., 1982, Trace element characteristics of lavas from destructive plate boundaries, in Thorpe, R.S., ed., *Andesites: Orogenic Andesites and Related Rocks*: Chichester, John Wiley and Sons, 525-548.

Reagan, M.K., Ishizuka, O., Stern, R.J., Kelley, K.A., Ohara, Y., Blichert-Toft, J., Bloomer, S.H., Cash, J., Fryer, P., Hanan, B.B., and Hickey-Vargas, R., 2010, Fore-arc basalts and subduction initiation in the Izu-Bonin-Mariana system: *Geochemistry, Geophysics, Geosystems*, 11, doi:10.1029/2009GC002871.

Rinehart, C.D., and Ross, D.C., 1957, Geologic map of the Casa Diablo Mountain Quadrangle, California: U.S. Geological Survey Map GQ99, scale 1:62,500.

Rinehart, C.D., and Ross, D.C., 1964, Geology and mineral deposits of the Mount Morrison quadrangle, Sierra Nevada, California: U.S. Geological Survey Professional Paper 385, 106 p.

Rinehart, C.D., Ross, D.C. and Huber, N.K., 1959, Paleozoic and Mesozoic fossils in a thick stratigraphic section in the eastern Sierra Nevada, California: *Geological Society of America Bulletin*, 70, 941-946.

Saleeby, J., 2011, Geochemical mapping of the Kings-Kaweah ophiolite belt, California - Evidence for progressive mélangé formation in a large offset transform subduction initiation environment, in Wakabayashi, J., and Dilek, Y., eds., *Mélanges: Processes of Formation and*

Societal Significance: Geological Society of America Special Paper 480,
doi:10.1130/2011.2480(02).

Saleeby, J.B., and Busby, C., 1993, Paleogeographic and tectonic setting of axial and western metamorphic framework rocks of the southern Sierra Nevada, California, in Dunne, G., and McDougall, K. (eds.), *Mesozoic Paleogeography of the Western United States II: SEPM, Pacific Section*, 197-226.

Saleeby, J.B., Kistler, R.W., Longiaru, S., Moore, J.G. and Nokleberg, W.J., 1990, Middle Cretaceous silicic metavolcanic rocks in the Kings Canyon area, central Sierra Nevada, California: *Geological Society of America Memoir 174*, 251-271.

Savage, J., Douglas, S.R., Barth, A.P., and Riggs, N.R., 2017, Geochemistry and facies of the eastern Sierra Nevada as analogues for modern continental arc settings: *GSA Abstracts with Programs*, 49, 7.

Sawka, W.N., Chappell, B.W., and Kistler, R.W., 1990, Granitoid compositional zoning by side-wall boundary layer differentiation: Evidence from the Palisade Crest Intrusive Suite, central Sierra Nevada, California: *Journal of Petrology*, 31, 519-553.

Schweickert, R.A., and Lahren, M.M., 1993, Triassic-Jurassic magmatic arc in eastern California and western Nevada: Arc evolution, cryptic tectonic breaks, and significance of the Mojave-Snow Lake fault, in Dunne, G., and McDougall, K., eds., *Mesozoic paleogeography of the western United States: Pacific Coast Paleogeography Symposium II: Pacific Section, SEPM (Society for Sedimentary Geology)*, 227-246.

Schweickert, R.A., and Lahren, M.M., 1999, Triassic caldera at Tioga Pass, Yosemite National Park, California: Structural relationships and significance: *Geological Society of America Bulletin*, 111, 1714-1722.

- Schweickert, R.A., and Lahren, M.M., 2006, Geologic evolution of Saddlebag Lake pendant, eastern Sierra Nevada, California: Tectonic implications, in Girty, G., and Cooper, J.D., eds., Using stratigraphy, sedimentology, and geochemistry to unravel the geologic history of the southwestern Cordillera: Pacific Section, SEPM (Society for Sedimentary Geology), 27-56.
- Sharp, W.D., Tobisch, O.T. and Renne, P.R., 2000, Development of Cretaceous transpressional cleavage synchronous with batholith emplacement, central Sierra Nevada, California: Geological Society of America Bulletin, 112, 1059-1066.
- Shukle, J.T., Barth, A.P., Wooden, J.L., Riggs, N.R., and Walker, J.D., 2016, Geochemistry and discriminant analysis of zircons from Triassic plutonic and volcanic rocks in the Sierra Nevada: Tracing the origins of granodiorite and ignimbrites following arc initiation: GSA Abstracts with Programs, 48, 7.
- Sorensen, S.S., Dunne, G.C., Hanson, R.B., Barton, M.D., Becker, J., Tobisch, O.T., and Fiske, R.S., 1998, From Jurassic shores to Cretaceous plutons: Geochemical evidence for paleoalteration environments of metavolcanic rocks, eastern California: Geological Society of America Bulletin, 110, 326-343.
- Stevens, C.H., and Greene, D.C., 1999, Stratigraphy, depositional history, and tectonic evolution of Paleozoic continental-margin rocks in roof pendants of the eastern Sierra Nevada, California: Geological Society of America Bulletin, 111, 919-933.
- Stevens, C.H., and Greene, D.C., 2000, Geology of Paleozoic rocks in eastern Sierra Nevada roof pendants, California, in Lageson, D.R., Peters, S.G., and Lahren, M.M. (eds.), Great Basin and Sierra Nevada: Boulder, Colorado, Geological Society of America Field Guide 2, 237-254.

Stone, P., and Stevens, C.H., 1988, Pennsylvanian and Early Permian paleogeography of east-central California: Implications for the shape of the continental margin and the timing of continental truncation: *Geology*, 16, 330-333.

Straub, S.M., Woodhead, J.D., and Arculus, R.J., 2015, Temporal evolution of the Mariana arc: Mantle wedge and subducted slab controls revealed with a tephra perspective: *Journal of Petrology*, 56, 409-439, doi: 10.1093/petrology/egv005.

Tamura, Y., Gill, J.B., Tollstrup, D., Kawabata, H., Shukuno, H., Chang, Q., Miyazaki, T., Takahashi, T., Hirahara, Y., Kodaira, S., Ishizuka, O., Suzuki, T., Kido, Y., Fiske, R.S., and Tatsumi, Y., 2009, Silicic magmas in the Izu-Bonin oceanic arc and implications for crustal evolution: *Journal of Petrology*, 50, 685-723.

Tani, K., Fiske, R.S., Tamura, Y., Kido, Y., Naka, J., Shukuno, H., and Takeuchi, R., 2008, Sumisu volcano, Izu-Bonin arc, Japan: site of a silicic caldera-forming eruption from a small open-ocean island: *Bulletin of Volcanology*, 70, 547-562.

Tikoff, B., and Greene, D., 1997, Stretching lineations in transpressional shear zones: an example from the Sierra Nevada Batholith, California: *Journal of Structural Geology*, 19, 29-39.

Tikoff, B., and Saint Blanquat, M., 1997, Transpressional shearing and strike-slip partitioning in the Late Cretaceous Sierra Nevada magmatic arc, California: *Tectonics*, 16, 442-459.

Tobisch, O.T., and Fiske, R.S., 1982, Repeated parallel deformation in part of the eastern Sierra Nevada, California and its implications for dating structural events: *Journal of Structural Geology*, 4, 177-195.

- Tobisch, O.T., Fiske, R.S., Sacks, S. and Taniguchi, D., 1977, Strain in metamorphosed volcaniclastic rocks and its bearing on the evolution of orogenic belts: Geological Society of America Bulletin, 88, 23-40.
- Tobisch, O.T., Saleeby, J.B., and Fiske, R.S., 1986, Structural history of continental volcanic arc rocks, eastern Sierra Nevada, California: A case for extensional tectonics: Tectonics, 5, 65-94.
- Tobisch, O.T., Fiske, R.S., Saleeby, J.B., Holt, E., and Sorensen, S.S., 2000, Steep tilting of metavolcanic rocks by multiple mechanisms, central Sierra Nevada, California: Geological Society of America Bulletin, 112, 1043-1058.
- Wright, I.C., Gamble, J.A., and Shane, P.A.R., 2003, Submarine silicic volcanism of the Healy caldera, southern Kermadec arc (SW Pacific): 1 – volcanology and eruption mechanisms: Bulletin of Volcanology, 65, 15-29.

Table 1. SIMS U-Pb zircon geochronology of Triassic and Jurassic tuffs in the Ritter Range and Mount Morrison pendants

Rock Unit	Sample#	SiO₂	Age (Ma)
<u>Ritter Range pendant</u>			
tuff of west Shadow Lake	14953	67.7%	167±2
tuff of lower Shadow Falls	14957	n.a.	168±2
tuff of upper Shadow Meadows	14949	75.3%	168.6±1
tuff of Rosalie Lake	14940	70.0%	169±2
tuff of lower Shadow Meadows	14950	73.8%	170.8±1
tuff of Olaine Lake	14961	n.a.	171±2
tuff	RR8943	n.a.	174±3
tuff	RR9033	n.a.	206±2
tuff of upper Shadow Falls (Little Pink)	14948	70.5%	207.3±1
tuff of San Joaquin Mountain (upper)	14964	70.7%	218±2

tuff of upper Shadow Falls (Little White)	14946	73.1%	219.0±1
tuff of upper Shadow Falls (Big Pink)	14947	74.8%	219±2
tuff of Agnew Meadows (lower)	14960	n.a.	220±2
tuff of Agnew Meadows (upper)	14962	n.a.	220±2
tuff of San Joaquin Mountain (lower)	14969	71.5%	220±2
tuff of San Joaquin Mountain (middle)	14967	74.6%	221±2

Mount Morrison pendant

tuff of Skelton Lake	11858	72.4%	216.5±1
----------------------	-------	-------	---------

n.a. - not analyzed

Accepted Article

FIGURE CAPTIONS

Figure 1. Geologic map showing plutonic rocks and pendants of the east-central Sierra Nevada and Mono Basin - northern Owens Valley region, adapted from Rinehart and Ross (1957), Bateman (1992), Huber and Rinehart (1965), Kistler (1966a, b), Crowder et al. (1972), Krauskopf and Bateman (1977), and Schweickert and Lahren (1999). MMP = Mount Morrison pendant, PCP = Pine Creek pendant, RRP = Ritter Range pendant, SLP = Saddlebag Lake pendant.

Figure 2. Geochronology sample location map, eastern Ritter Range pendant. See Figure 1 for location.

Figure 3. Geologic map, eastern Ritter Range pendant, adapted from unpublished mapping by R. Fiske. See Figure 1 for location. Rounded rectangles are SIMS zircon ages (in Ma) from this study, circles are TIMS zircon ages from Tobisch et al. (2000). Structural blocks shown at left are from Tobisch et al. (2000).

Figure 4. Stratigraphic column for volcanic rocks of the Koip sequence in the Ritter Range pendant. Numbers to the right locate ignimbrites with Pb/U zircon ages in Ma. SIMS ages from this study and TIMS ages from Tobisch et al. (2000). 'EJR' locates limestone interval with Early Jurassic fossil age from Rinehart et al. (1959).

Figure 5. Tuffs are deformed and weakly regionally metamorphosed (Tobisch et al., 1977) but primary igneous textures are commonly well-preserved. Finite strain is heterogeneous, with *average* shortening ~30 to 50% but porphyritic textures are well preserved in low strain zones. A, B. Photomicrographs of porphyritic Jurassic tuff of Rosalie Lake with euhedral, weakly internally-deformed quartz and feldspar phenocrysts. C, D. Photomicrographs of porphyritic

Triassic tuffs of upper Shadow Falls and Agnew Meadows with subhedral quartz and feldspar phenocrysts. Field of view ~1mm across in all photomicrographs.

Figure 6. Zircon spot analyses and weighted mean $^{206}\text{Pb}^*/^{238}\text{U}$ ages for rocks of the eastern Ritter Range pendant. Individual zircon ages are plotted as 2σ error bars. Weighted mean ages, interpreted as the crystallization age, are shown with associated 2σ errors. Zircon spot analyses plotted with lightly-shaded error bars were excluded from the age calculation.

Figure 7. Zircon age summary for extrusive rocks from pendants in the early Mesozoic east Sierran arc and for plutons of adjacent intrusive suites. Solid diamonds are SIMS weighted mean $^{206}\text{Pb}^*/^{238}\text{U}$ zircon ages (with 2σ errors); open diamonds are TIMS zircon ages. Additional TIMS data are from Saleeby et al. (1990), Tobisch et al. (2000), Mahan et al. (2003), and additional SIMS and TIMS data from Barth et al. (2011, 2014). Timing of magmatic pulses (*p1*, *p2*) and intervening lull (*II*) in the California arc from Barth et al. (2013).

Figure 8. Whole rock potassium, titanium and aluminum contents as a function of silica content of early Mesozoic tuffs of the eastern Ritter Range. Analyses of tuffs of Davis Lakes and Nydiver Lakes and additional data for the tuff of Rosalie Lake are from Sorensen et al. (1998); Saddlebag Lake pendant Triassic tuffs from Barth et al. (2012).

Figure 9. Whole rock trace element abundances in dacitic to rhyolitic tuffs of the eastern Ritter Range, normalized to primitive mantle (McDonough and Sun, 1995). Symbols as in Figure 8. Tuffs are compared to Oligocene dacite to rhyolite whole rocks and glasses from the early Izu-Bonin arc (IB; Ishizuka et al., 2011; Brandl et al., 2017).

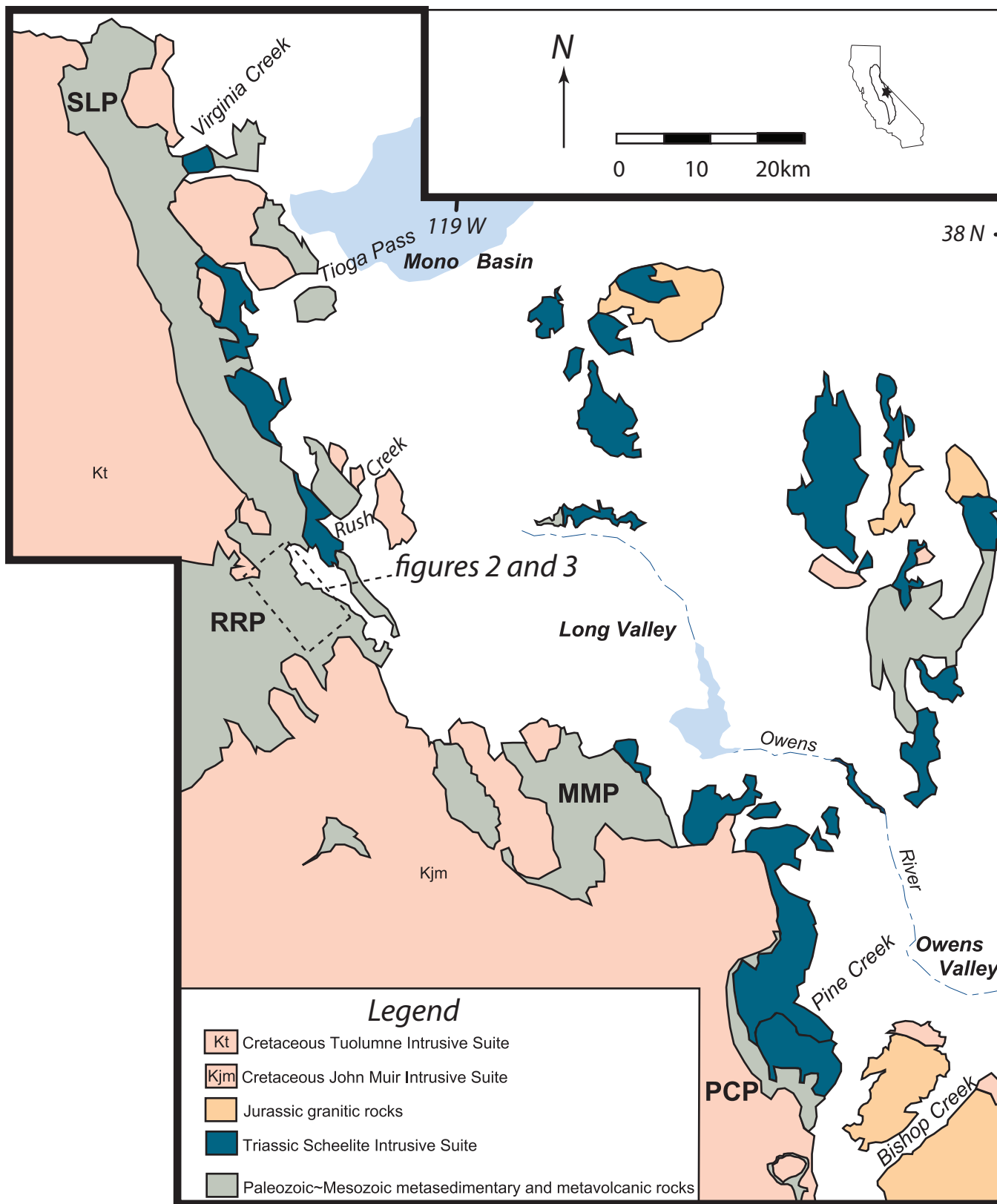
Figure 10. Hf and Ti abundances and Ce/U in Triassic and Jurassic magmatic zircons from Ritter Range tuffs. Note that zircons have similar ranges in Hf and show decreasing Ce/U and Ti

with fractionation. Triassic zircons are relatively depleted in Ti and have lower average Ce/U. Saddlebag Lake data are from Barth et al. (2012) and Shukle et al. (2016).

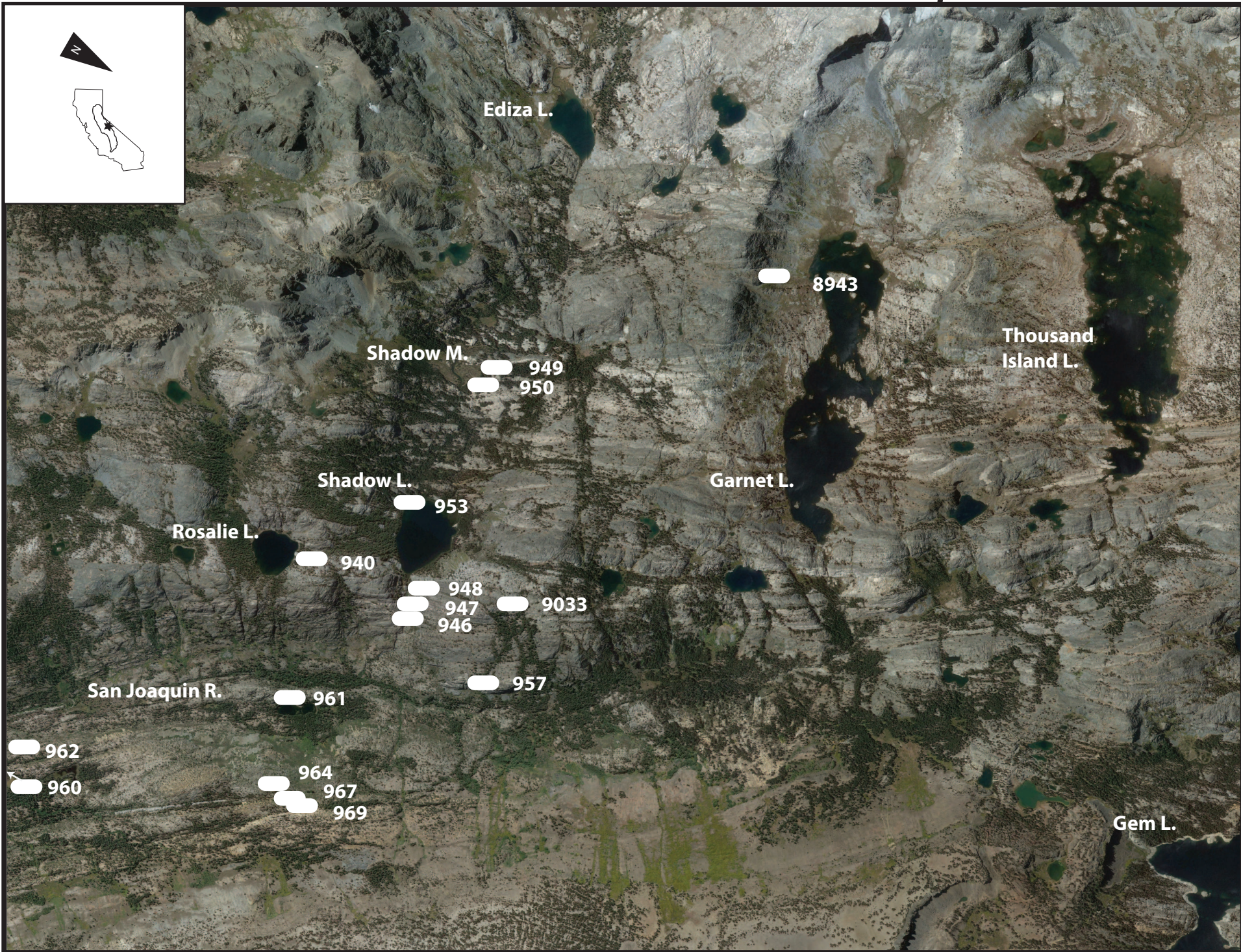
Figure 11. Th/U and Ce/Yb variations in magmatic zircons. Triassic zircons in tuffs from the Ritter Range, Saddlebag Lake and Mount Morrison pendants that have low average Th/U are relatively depleted in Ce and Th. Note that the youngest Triassic samples are transitional in character. Saddlebag Lake data are from Barth et al. (2012) and Shukle et al. (2016).

Figure 12. Scandium and Uranium enrichment in oceanic arc and Sierran zircons compared to modern mid-ocean ridge, back-arc basin, and intraplate magmatic zircons. Data sources: mid-ocean ridge zircons from Grimes et al. (2009); intraplate zircons from Carley et al. (2011); back-arc basin and oceanic arc zircons from Barth et al. (2017).

Figure 13. (A, B) Uranium enrichment in arc zircons (Claiborne, 2011; Coombs and Vazquez, 2014; Dilles et al., 2015; Barth et al., 2017). The well-known lithophile element enrichment of arc lavas from convergent margin settings is reflected in relative U enrichment in zircons, where low to high U/Yb zircons formed in low to high K silicic arc melts. (C, D) Nb/Yb vs. U/Yb diagram illustrating slab-related non-conservative behavior of arc-derived zircons relative to non-slab-related mantle enrichment. Main MOR – OI array is based on mid-ocean ridge zircons from the Mid-Atlantic and Indian ridges (Grimes et al., 2009) and ocean island zircons from Iceland (Carley et al., 2011).



37.7 N

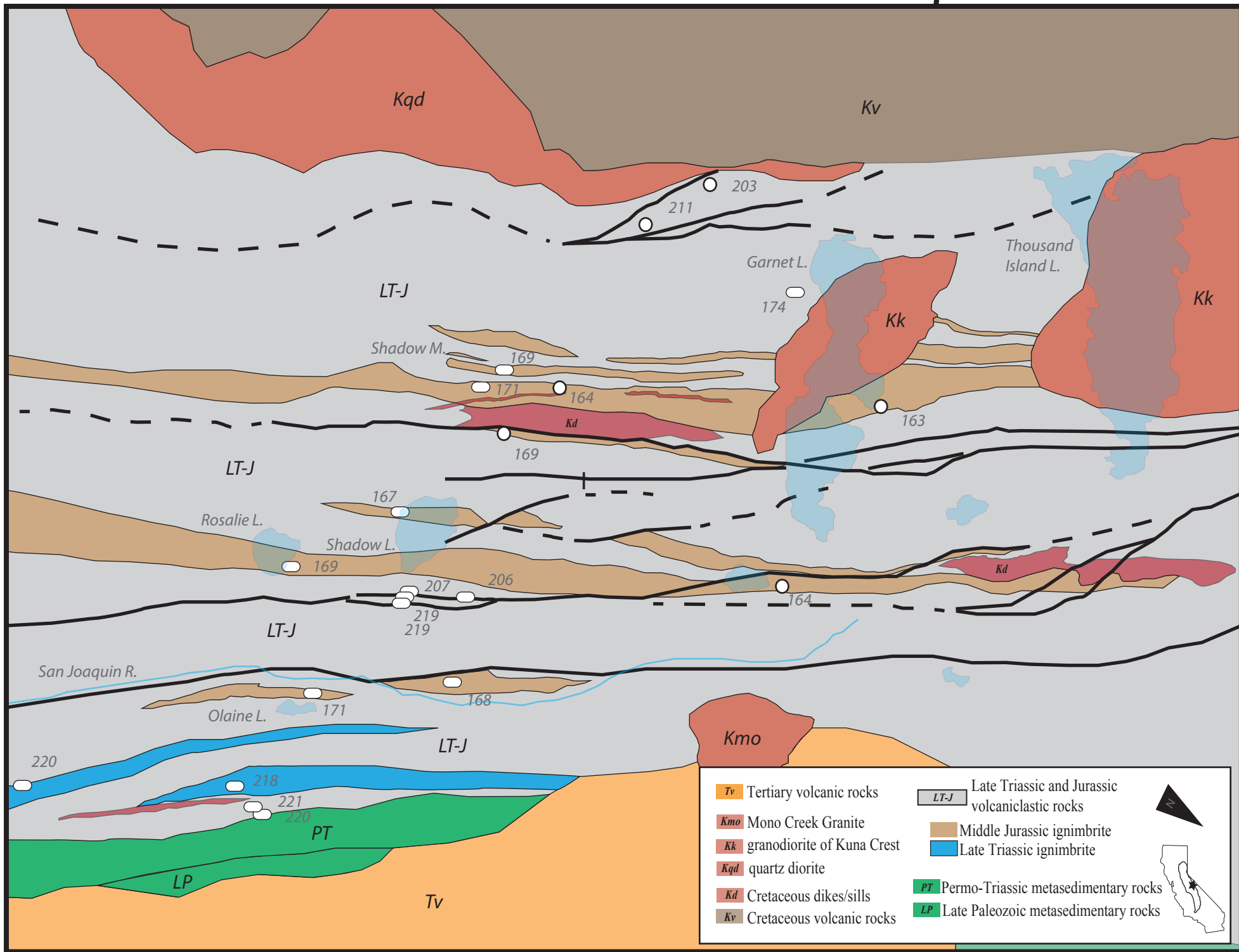


37.7 N

III, IV



37.7 N



Tv Tertiary volcanic rocks	LT-J Late Triassic and Jurassic volcanoclastic rocks
Kmo Mono Creek Granite	Middle Jurassic ignimbrite
Kk granodiorite of Kuna Crest	Late Triassic ignimbrite
Kqd quartz diorite	PT Permo-Triassic metasedimentary rocks
Kd Cretaceous dikes/sills	LP Late Paleozoic metasedimentary rocks
Kv Cretaceous volcanic rocks	

A north arrow pointing upwards and an inset map of California with a star indicating the location of the study area.

37.7 N

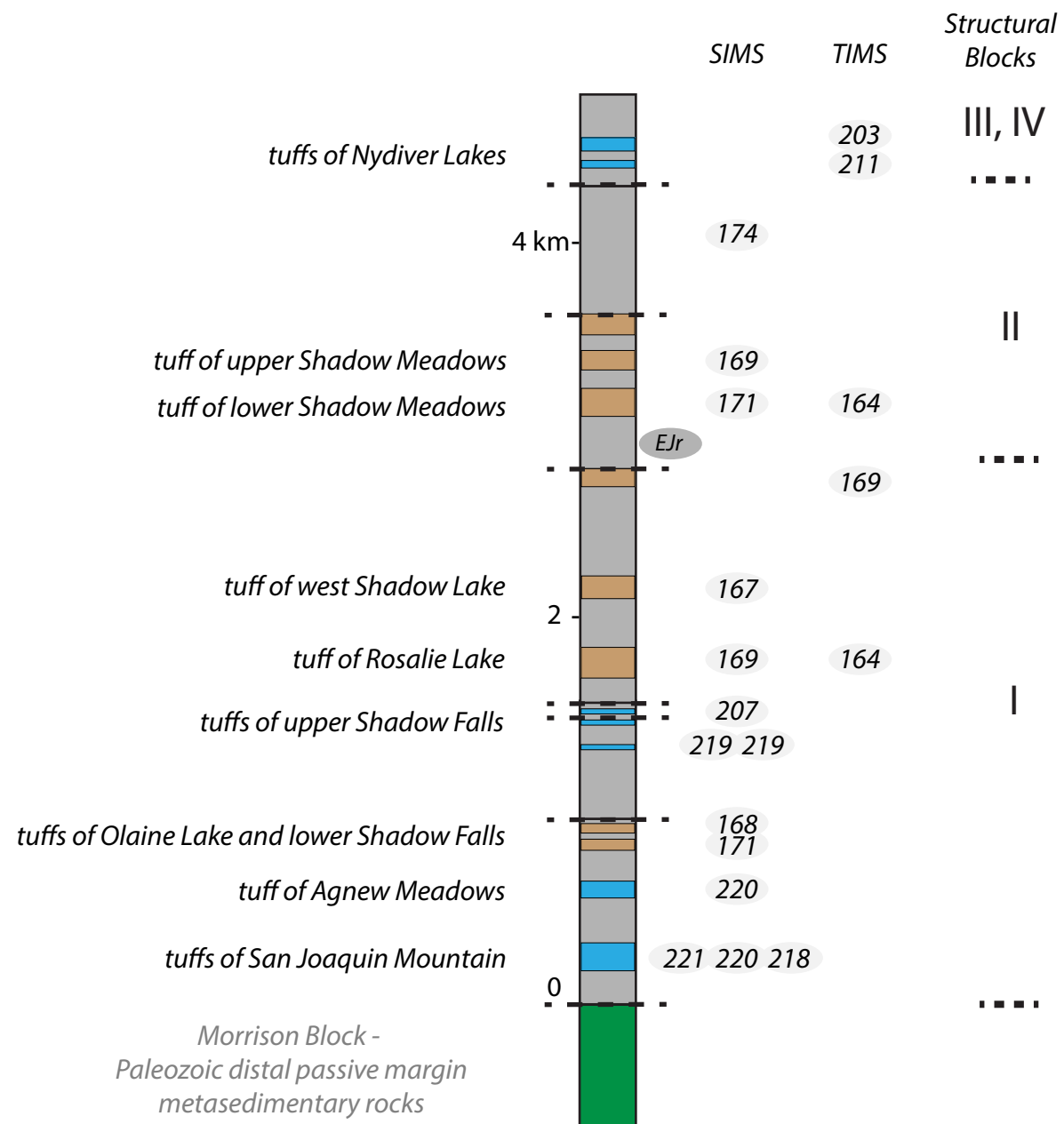


Figure 5

